not observed after electrooxidation of (P)In[$N_4C(R)$], as is the case for (P)In(R). In addition, half-wave potentials for the first reduction and first oxidation of (P)In[$N_4C(R)$] are not close to those of the σ-bonded carbon derivatives but rather are similar to those of ionic (P)InX species.[61] Moreover, as already noted, the UV-visible spectra of (P)In[$N_4C(R)$] are close to those of the ionic (P)InX derivatives.

Numerous correlations have been made between the redox and spectral properties of different metalloporphyrins. For example, the degree of axial-bond polarization has been related to the ratio of Q band molar absorptivity, $\epsilon(\alpha)/\epsilon(\beta)$, in the UV-visible spectra. This ratio is listed in Table XIV for indium tetraphenylporphyrin complexes with different axial ligands, and the resulting correlation between $E_{1/2}$ and spectral data is graphically presented in Figure 10. The value of $\epsilon(\alpha)/\epsilon(\beta)$ for (TPP)In[$N_4C(C_6H_5)$] is 0.47 and is similar to values measured for (TPP)InX where X = SO_3Ph^-, SO_3Me^-, Cl^-, OAc^-, N_3^-, CN^-, or ClO_4^- (see Table XIV). In contrast, the $\epsilon(\alpha)/\epsilon(\beta)$ ratios for the (P)In(R) complexes reflect a changeover of the metal-ligand bond from pure σ-bonded character when R = $C(CH_3)_3$ or $CH(CH_3)_2$ to an ionic-like character when R = $C_2C_6H_5$. This is reflected by the data in Figure 10, which clearly demonstrates that the tetrazolato and triazolato complexes both have an axial indium-nitrogen bond with ionic-like character.

Acknowledgment. The support of the CNRS, the National Science Foundation (Grants CHE-8515411 and INT-8412696), and NATO (Grant 0168/87) is gratefully acknowledged.

Supplementary Material Available: Tables of hydrogen atom fractional coordinates, anisotropic temperature factors, bond distances and angles, and least-squares planes (13 pages); a table of observed and calculated structure factors for (OEP)In[$N_4C(CH_3)$] (26 pages). Ordering information is given on any current masthead page.

Contribution from the Laboratoire de Synthèse et d'Electrosynthèse Organométalliques, associé au CNRS (URA 33), Faculté des Sciences "Gabriel", 6, Boulevard Gabriel, 21100 Dijon, France, Department of Chemistry, University of Houston, Houston, Texas 77204-5641, and Laboratoire de Minéralogie et Cristallographie associé au CNRS (URA 809), Université de Nancy I, BP 239, 54506 Vandoeuvre les Nancy, France

Metalloporphyrins Containing σ-Bonded Nitrogen Axial Ligands. 2. Synthesis and Characterization of Iron(III) Tetrazolato and Triazolato Porphyrin Complexes. Molecular Structure of (5-Methyltetrazolato)(2,3,7,8,12,13,17,18-octaethylporphinato)iron(III)

R. Guilard,*[1a] I. Perrot,[1a,b] A. Tabard,[1a] P. Richard,[1a] C. Lecomte,[1c] Y. H. Liu,[1b] and K. M. Kadish*[1b]

Received June 11, 1990

The first synthesis and characterization of iron(III) porphyrins with σ-bonded tetrazolato or triazolato axial ligands are reported. These compounds are represented as (P)Fe[$N_4C(R)$] or (P)Fe($N_3C_6H_4$) where P = the dianion of octaethylporphyrin (OEP) or tetramesitylporphyrin (TMP) and R = C_6H_5, *p*-$CH_3C_6H_4$, *m*-$CH_3C_6H_4$, CH_3, or CH_2CH_3. Each metalloporphyrin may exist in two different isomeric forms, which are labeled as isomer I and isomer II for the case of (P)Fe[$N_4C(R)$]. The linkage mode of the tetrazolato group (and the type of isomer) was determined for two representative complexes by single-crystal X-ray diffraction. (OEP)Fe[$N_4C(CH_3)$]·$^1/_2C_6H_5CH_3$ crystallizes as isomer I in the monoclinic system, space group $P2_1/c$ (a = 15.967 (2) Å, b = 17.464 (4) Å, c = 14.726 (2) Å, β = 66.59 (2)°, Z = 4, V = 3765 Å^3, ρ = 1.27 g cm^{-3}, $R(F)$ = 5.97%, $R_w(F)$ = 5.82%). (OEP)Fe[$N_4C(C_6H_5)$] also crystallizes in the monoclinic space system, space group $P2_1/c$ (a = 12.798 (2) Å, b = 12.748 (3) Å, c = 24.301 (5) Å, β = 78.93 (2)°, Z = 4, V = 3891 Å^3, ρ = 1.25 cm^{-3}) but exists as isomer II. Altogether, eight different tetrazolato and triazolato complexes were synthesized, and each was characterized by UV-visible, IR, ESR, and ^{1}H NMR spectroscopy, as well as by electrochemistry. Variable-temperature magnetic susceptibility measurements were also performed and give data consistent with a high-spin-state Fe(III) central metal. An analysis of the isotropic chemical shifts shows that the electronic structures of the high-spin-state complexes are virtually independent of the specific σ-bonded nitrogen axial ligand.

Introduction

Numerous papers have been devoted to a characterization of organic and inorganic azide reactivity. Organic azides can react with nitriles, alkenes, or alkynes to give tetrazoles, triazolines, or triazoles,[2-5] while inorganic azides can react with dipolarophiles to give as a final product a metal-nitrogen-bonded heterocycle.[6-22]

Chart I

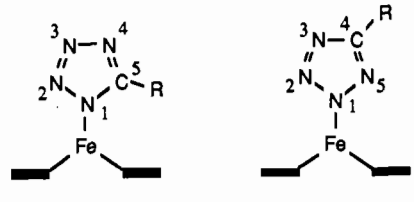

ISOMER I ISOMER II

Recently, these classical reactions have been utilized to synthesize main-group or transition-metal metalloporphyrins with σ-bonded

(1) (a) Université de Bourgogne. (b) University of Houston. (c) Université de Nancy I.
(2) L'Abbé G. *Chem. Rev.* **1969**, *69*, 345 and references therein.
(3) Patai, S. *The Chemistry of Azido Group*; Interscience: New York, 1971.
(4) Huisgen, R. In *1,3-Dipolar Cycloaddition Chemistry*; Padwa, A., Ed.; Interscience: New York, 1984; Vol. I, Chapter I.
(5) Scriven, E. F. V. *Azides and Nitrenes, Reactivity and Utility*; Academic: Orlando, FL, 1984.
(6) Beck, W.; Fehlhammer, W. P. *Angew. Chem., Int. Ed. Engl.* **1967**, *6*, 169.
(7) Beck, W.; Fehlhammer, W. P.; Bock, H.; Bauder, M. *Chem. Ber.* **1969**, *102*, 3637.
(8) Beck, W.; Burger, K.; Fehlhammer, W. P. *Chem. Ber.* **1971**, *104*, 1816.
(9) Weis, J. C.; Beck, W. *Chem. Ber.* **1972**, 105, 3203.
(10) Fehlhammer, W. P.; Kemmerich, T.; Beck, W. *Chem. Ber.* **1979**, *112*, 468.
(11) Kreutzer, P. H.; Weis, J. C.; Bock, H.; Erbe, J.; Beck, W. *Chem. Ber.* **1983**, *116*, 2691.
(12) Fehlhammer, W. P.; Beck, W. *Z. Naturforsch.* **1983**, *38B*, 546.
(13) Ziolo, R. F.; Thich, J. A.; Dori, Z. *Inorg. Chem.* **1972**, *11*, 626.
(14) Dori, Z.; Ziolo, R. F. *Chem. Rev.* **1973**, *73*, 247.
(15) (a) Sato, F.; Etoh, M.; Sato, M. *J. Organomet. Chem.* **1972**, *37*, C51. (b) *Ibid.* **1974**, *70*, 101.
(16) Rosan, A.; Rosenblum, M. *J. Organomet. Chem.* **1974**, *80*, 103.
(17) Busetto, L.; Palazzi, A.; Ros, R. *Inorg. Chim. Acta* **1975**, *13*, 233.
(18) Rigby, W.; Bailey, P. M.; McCleverty, J. A.; Maitlis, P. M. *J. Chem. Soc., Dalton Trans.* **1979**, 371.
(19) La Monica, G.; Ardizzoia, G.; Cenini, S.; Porta, F. *J. Organomet. Chem.* **1984**, *273*, 263.

0020-1669/91/1330-0027$02.50/0

Table I. Reaction Conditions for Synthesis of Investigated Complexes

porphyrin, P	axial ligand	reacn temp, °C	reacn time, h	recrystn solvent	yield, %
OEP	$N_4C(C_6H_5)$	85	15	toluene	63
	$N_4C(p\text{-}CH_3C_6H_4)$	85	15	toluene	63
	$N_4C(m\text{-}CH_3C_6H_4)$	85	15	toluene/ heptane	60
	$N_4C(CH_3)$	130	72	toluene	75
	$N_4C(CH_2CH_3)$	130	48	toluene	46
	$N_3C_6H_4$	121	15	*a*	50
TMP	$N_4C(C_6H_5)$	85	15	*b*	60
	$N_4C(CH_3)$	130	72	*b*	55

[a] Crude product. [b] Compound could not be recrystallized due to its high solubility in all investigated solvents.

tetrazolato or triazolato axial ligands. The formation of these complexes proceeds via a cycloaddition reaction involving organic nitriles or alkynes and an azido metalloporphyrin of the type $(P)MN_3$ or $(P)M(N_3)_2$ where P = the dianion of a given porphyrin ring and M = Co,[23] Ge,[24] Sn,[24] or In.[25,26]

The thermal decomposition of iron porphyrin azides has been the focus of many experimental and theoretical studies,[27-36] but the use of this complex as a starting material to synthesize iron(III) porphyrins with σ-bonded nitrogen axial ligands has never been reported. This has now been accomplished and is described in the present paper, which presents the first synthesis and characterization of iron(III) porphyrins with σ-bonded tetrazolato or triazolato axial ligands. These compounds are represented by $(P)Fe[N_4C(R)]$ or $(P)Fe(N_3C_6H_4)$ where P = the dianion of octaethylporphyrin (OEP) or tetramesitylporphyrin (TMP) and R = C_6H_5, $p\text{-}CH_3C_6H_4$, $m\text{-}CH_3C_6H_4$, CH_3, or CH_2CH_3.

Two different substitution isomers labeled as I and II are possible for each $(P)Fe[N_4C(R)]$ metalloporphyrin, and these are shown in Chart I.

It was of special interest to determine which isomer is formed for $(P)Fe[N_4C(R)]$ complexes with different axial-substituted tetrazolato ligands, since recent structure determinations for phenylimidazole-inhibited complexes of cytochrome P-450$_{cam}$ have demonstrated that each investigated imidazole inhibitor (1- or 4-phenylimidazole), except for 2-phenylimidazole, was bonded to the heme iron via the ligand nitrogen atom.[37] Steric repulsion was invoked to explain the lack of coordination with 2-phenylimidazole, and a comparison of structural data for $(OEP)Fe[N_4C(C_6H_5)]$ and $(OEP)Fe[N_4C(CH_3)]$ in this present paper confirms this hypothesis.

Table II. Unit Cell Parameters for $(OEP)In[N_4C(C_6H_5)]$ and $(OEP)Fe[N_4C(C_6H_5)]$

compd	$(OEP)In[N_4C(C_6H_5)]$	$(OEP)Fe[N_4C(C_6H_5)]$
formula	$C_{43}H_{49}N_8In$	$C_{43}H_{49}N_8Fe$
fw	792.77	733.77
space group	$P2_1/c$	$P2_1/c$
lattice params		
a, *b*, *c*, Å	12.897 (2), 12.695 (9), 24.50 (2)	12.798 (2), 12.748 (3), 24.301 (5)
β, deg	79.26 (3)	78.93 (2)
V, Å^3; Z; ρ_{calcd}, g cm^{-3}	3942; 4; 1.34	3891; 4; 1.25
diffractometer	Enraf-Nonius CAD 4 F (room temp)	Enraf-Nonius CAD 4 F (room temp)

Altogether, eight different (tetrazolato)- and (triazolato)iron(III) complexes were synthesized, and each was characterized by UV–visible, infrared, ^{1}H NMR, and magnetic measurements, as well as by electrochemistry. These data were analyzed with respect to the isomer type, which was verified by a single-crystal X-ray diffraction study of two representative compounds in the tetrazolato series. The overall results are compared to data for the analogous In(III) tetrazolato and triazolato complexes[26] as well as to data for other Fe(III) porphyrins of the types (P)Fe(R) and (P)FeX where R is a σ-bonded axial ligand and X is an anionic axial ligand such as Cl^- or Br^-.

Experimental Section

Chemicals. The synthesis and handling of each triazolato or tetrazolato complex were carried out under an argon atmosphere. Common solvents were distilled under argon and thoroughly dried prior to use. All synthetic operations were carried out in Schlenk tubes. Acetonitrile (CH_3CN), propionitrile (CH_3CH_2CN), benzonitrile (C_6H_5CN), *m*-tolunitrile ($m\text{-}CH_3C_6H_4CN$), and *p*-tolunitrile ($p\text{-}CH_3C_6H_4CN$) were freshly distilled under an inert atmosphere. Methylene chloride (CH_2Cl_2) was distilled over P_2O_5. Tetra-*n*-butylammonium perchlorate ((TBA)ClO_4) and tetra-*n*-butylammonium hexafluorophosphate ((TBA)PF_6) were purchased from Fluka Corp. and recrystallized first from absolute ethanol and then from ethyl acetate, after which they were dried in a vacuum oven at 40 °C. Benzyne was prepared in situ by using literature methods.[38,39] (P)FeCl was synthesized as described in the literature.[40] $(P)FeN_3$ was synthesized from a reaction involving (P)FeCl and NaN_3. Procedures for the preparation of $(P)FeN_3$, $(P)Fe[N_4C(R)]$, and $(P)Fe(N_3C_6H_4)$ are given below, while yields and reaction conditions are summarized in Table I.

Synthesis of $(P)FeN_3$ Where P = OEP or TMP. NaN_3 (189 mmol) was added to a solution of (P)FeCl (5.68 mmol) in methylene chloride (350 cm^3) and the reaction mixture refluxed for 12 h with stirring. The solution was then filtered and the solvent removed under vacuum. The crude product was recrystallized from a mixture of toluene and heptane and gave an overall yield close to 95%.

Synthesis of $(P)Fe[N_4C(R)]$ Where P = OEP or TMP and R = C_6H_5, $m\text{-}CH_3C_6H_4$, or $p\text{-}CH_3C_6H_4$. A solution of $(P)FeN_3$ (0.45 mmol) in benzonitrile, *m*-tolunitrile, or *p*-tolunitrile (80 cm^3) was heated at 85 °C for 15 h as the progress of the reaction was monitored by UV–visible spectroscopy. The nitrile was removed under vacuum and the crude product of $(OEP)Fe[N_4C(R)]$ recrystallized from toluene or a a toluene/heptane mixture. $(TMP)Fe[N_4C(C_6H_5)]$ could not be recrystallized due to its high solubility in all solvents.

Synthesis of $(P)Fe[N_4C(R)]$ Where P = OEP or TMP and R = CH_3 or CH_2CH_3. $(P)FeN_3$ (0.45 mmol) was dissolved in a mixture of xylene/acetonitrile or xylene/propionitrile (1/3, 80 cm^3) and refluxed for 72 h as the progress of the reaction was monitored by UV–visible spectroscopy. The crude product of $(OEP)Fe[N_4C(R)]$ was isolated and purified according to the above procedure. Again, the TMP derivative could not be recrystallized due to its high solubility.

Synthesis of $(OEP)Fe(N_3C_6H_4)$. A monoglyme solution (10 cm^3) of anthranilic acid (0.48 mmol) was added dropwise to $(OEP)FeN_3$ (0.32 mmol) and isoamyl nitrite (0.48 mmol) in monoglyme (50 cm^3). The solution mixture was refluxed for 15 h while the resulting product was

(20) Kreutzer, P.; Weis, J. C.; Boehme, H.; Kemmerich, T.; Beck, W.; Spencer, C.; Mason, R. *Z. Naturforsch.* **1972**, *27B*, 745.
(21) Kemmerich, T.; Nelson, J. H.; Takach, N. E.; Boehme, H.; Jablonski, B.; Beck, W. *Inorg. Chem.* **1982**, *21*, 1226.
(22) Paul, P.; Nag, K. *Inorg. Chem.* **1987**, *26*, 2969.
(23) Geisenberger, J.; Erbe, J.; Heidrich, J.; Nagel, U.; Beck, W. *Z. Naturforsch.* **1987**, *42B*, 55.
(24) Jagerovic, N.; Barbe, J.-M.; Farnier, M.; Guilard, R. *J. Chem. Soc., Dalton Trans.* **1988**, 2569.
(25) Guilard, R.; Gerges, S. S.; Tabard, A.; Richard, P.; El Borai, M. A.; Lecomte, C. *J. Am. Chem. Soc.* **1987**, *109*, 7228.
(26) Guilard, R.; Jagerovic, N.; Tabard, A.; Richard, P.; Courthaudon, L.; Louati, A.; Lecomte, C.; Kadish, K. M. *Inorg. Chem.*, preceding paper in this issue.
(27) Summerville, D. A.; Cohen, I. A. *J. Am. Chem. Soc.* **1976**, *98*, 1747.
(28) Scheidt, W. R.; Summerville, D. A.; Cohen, I. A. *J. Am. Chem. Soc.* **1976**, *98*, 6623.
(29) Kadish, K. M.; Bottomley, L. A.; Brace, J. G.; Winograd, N. *J. Am. Chem. Soc.* **1980**, *102*, 4341.
(30) Schick, G. A.; Bocian, D. F. *J. Am. Chem. Soc.* **1980**, *102*, 7982.
(31) Schick, G. A.; Bocian, D. F. *J. Am. Chem. Soc.* **1983**, *105*, 1830.
(32) Schick, G. A.; Findsen, E. W.; Bocian, D. F. *Inorg. Chem.* **1982**, *21*, 2885.
(33) Bocian, D. F.; Findsen, E. W.; Hofman, J. A., Jr.; Schick, G. A.; English, D. R.; Hendrickson, D. N.; Suslick, K. S. *Inorg. Chem.* **1984**, *23*, 800.
(34) Kadish, K. M.; Rhodes, R. K.; Bottomley, L. A.; Goff, H. M. *Inorg. Chem.* **1981**, *20*, 3195.
(35) Bottomley, L. A.; Garrett, B. B. *Inorg. Chem.* **1982**, *21*, 1260.
(36) Tatsumi, K.; Hoffman, R. *J. Am. Chem. Soc.* **1981**, *103*, 3328.
(37) (a) Poulos, T. L.; Howard, A. J. *Biochemistry* **1987**, *26*, 8165. (b) Bode, W.; Meyer, E., Jr.; Powers, J. C. *Biochemistry* **1989**, *28*, 1951.
(38) Dougherty, C. M.; Baumgarten, R. L.; Sweeney, A., Jr.; Concepcion, E. *J. Chem. Educ.* **1977**, *54*, 643.
(39) Banks, R. E.; Higgons, R. I.; Prakash, A.; Rawstron, M.; Sparkes, G. R. *J. Fluorine Chem.* **1977**, *9*, 327.
(40) Buchler, J. W. In *The Porphyrins*; Dolphin, D., Ed.; Academic: New York, 1978; Vol. I, Chapter 10.

Table III. Crystallographic Data for (OEP)Fe[$N_4C(CH_3)$]·$^1/_2C_6H_5CH_3$

formula	$C_{41.5}H_{51}N_8Fe$
fw	717.77
space group	$P2_1/c$
lattice params	
a, b, c, Å	15.967 (2), 17.464 (4), 14.726 (2)
β, deg	66.59 (2)
V, Å^3; Z; ρ_{calcd}, g cm^{-3}	3765; 4; 1.27
$F(000)$	1528
diffractometer	Enraf-Nonius CAD 4 F (room temp)
radiation	Mo Kα
scan type; $(\sin\theta_{max})/\lambda$, Å^{-1}	ω–2θ; 0.6
scan range, deg; scan speed, deg min^{-1}	1 + 0.347 tan θ; 0.5 < v <2.7
aperture, mm	2 + 2 tan θ
hkl limits	$0 \le h \le 19$; $0 \le k \le 20$; $-17 \le l \le 17$
no. of reflns measd	4007
no. of reflns used (N)	1126
no. of params (N_p)	201
N/N_p	5.6
program used	SDP,[41] SHELX 76[42]
$R(F)$, %	5.97
$R_w(F)$, %	5.82
GOF	1.77

periodically monitored by UV–visible spectroscopy. The solvent was then evaporated under reduced pressure, after which the crude product was dissolved in toluene and precipitated by addition of heptane.

Instrumentation. ^{1}H NMR spectra were recorded at 400 MHz on a Bruker WM 400 spectrometer of CEREMA (Centre de Résonance Magnétique de l'Université de Bourgogne). Spectra were measured from 5-mg solutions of the complex in deuterated solvents with tetramethylsilane as internal reference. ESR spectra were recorded in toluene at 100 K on a Bruker ESP 300 spectrometer. The g values were measured with respect to diphenylpicrylhydrazyl (g = 2.0036 ± 0.0003). Magnetic measurements were obtained from a Foner magnetometer by using 50 mg of solid sample. Infrared spectra were obtained on a Perkin-Elmer 580 B apparatus. Solid samples were prepared as a 1% dispersion in CsI. Electronic absorption spectra were recorded on a Perkin-Elmer 559 spectrophotometer, an IBM Model 9430 spectrophotometer, or a Tracor Northern 6500 spectrometer.

Cyclic voltammograms were obtained with the use of a three-electrode system. The working electrode was a platinum button. A platinum wire served as the counter electrode, and the reference electrode was a saturated calomel electrode (SCE) that was separated from the bulk of the solution by a fritted-glass bridge.

Crystal Data for (OEP)Fe[$N_4C(C_6H_5)$] and X-ray Structure of (OEP)Fe[$N_4C(CH_3)$]·$^1/_2C_6H_5CH_3$. Unit cells and space groups were determined and checked by means of a short data collection on a CAD 4 Enraf-Nonius diffractometer with Mo Kα radiation. Unit cell parameters were obtained from least-squares refinement on the setting angles of 25 reflections (θ < 20°).

(OEP)Fe[$N_4C(C_6H_5)$] crystallizes in the monoclinic system space group $P2_1/c$. Unit cell parameters are given in Table II, which also includes data for (OEP)In[$N_4C(C_6H_5)$].[25] The two compounds are isomorphous, and no further data collection was made on the Fe(III) derivative.

Crystals of (OEP)Fe[$N_4C(CH_3)$] larger than 30 × 20 × 110 μm^3 could not be obtained, and such a small crystal was therefore utilized for the structural determination. The space group of this complex is monoclinic $P2_1/c$. Of 4007 reflections collected up to $(\sin\theta)/\lambda$ = 0.6 Å^{-1}, only 1126 reflections with $I \ge 3\sigma(I)$ were used to solve and refine the structure. Intensities were corrected for Lorentz and polarization effects (SDP).[41] The structure was solved by interpretation of the Patterson map and refined via standard least-squares techniques (SHELX 76).[42] Experimental details are given in Table III. The scattering factors were taken from refs 42 and 43. Due to the lack of data, only the iron atom was refined anisotropically. During refinement, difference electron density maps showed a large region of positive electron density near the ($^1/_2$, 0, $^1/_2$) inversion center. This result was interpreted as a disordered toluene solvent molecule in two different positions related by the inversion center. The geometry of the six atoms of the toluene ring (C50···C55) was idealized (C–C = 1.40 Å; C–C–C = 120°; fixed occu-

(41) *SDP: Structure Determination Package*; Enraf-Nonius: Delft, The Netherlands, 1977.
(42) Sheldrick, G. M. *SHELX-76: Program for Crystal Structure Determinations*; University of Göttingen: Göttingen, FRG, 1976.
(43) *International Tables for X-Ray Crystallography*; Kynoch: Birmingham, U.K., 1974; Vol. IV.

Table IV. Fractional Coordinates, Deviations, and Equivalent Isotropic Temperature Parameters (Å^2) of (OEP)Fe[$N_4C(CH_3)$]

atom	x	y	z	B
Fe	0.1708 (2)	−0.0713 (1)	0.1393 (3)	2.57 (7)
N1	0.175 (1)	−0.0979 (8)	0.272 (1)	2.4 (4)
N2	0.308 (1)	−0.0972 (8)	0.076 (1)	2.9 (4)
N3	0.164 (1)	−0.0951 (7)	0.007 (1)	2.1 (4)
N4	0.0333 (9)	−0.0895 (8)	0.205 (1)	2.2 (4)
N5	0.185 (1)	0.0441 (6)	0.136 (1)	2.0 (3)
N6	0.219 (1)	0.164 (1)	0.136 (1)	4.7 (4)
N7	0.215 (1)	0.146 (1)	0.048 (1)	5.2 (4)
N8	0.194 (1)	0.074 (1)	0.044 (1)	4.0 (4)
C1	0.102 (1)	−0.098 (1)	0.362 (1)	2.6 (5)
C2	0.138 (2)	−0.104 (1)	0.439 (2)	3.7 (5)
C3	0.227 (1)	−0.111 (1)	0.396 (1)	2.6 (5)
C4	0.253 (1)	−0.104 (1)	0.292 (2)	3.7 (5)
C5	0.340 (1)	−0.105 (1)	0.222 (2)	3.1 (5)
C6	0.368 (1)	−0.102 (1)	0.122 (2)	3.3 (5)
C7	0.459 (1)	−0.103 (1)	0.049 (1)	2.6 (5)
C8	0.457 (1)	−0.100 (1)	−0.040 (2)	2.3 (4)
C9	0.361 (1)	−0.096 (1)	−0.023 (1)	2.6 (5)
C10	0.327 (1)	−0.093 (1)	−0.096 (1)	3.3 (5)
C11	0.238 (1)	−0.096 (1)	−0.085 (2)	3.1 (5)
C12	0.205 (1)	−0.1032 (9)	−0.163 (1)	2.0 (4)
C13	0.115 (1)	−0.105 (1)	−0.119 (1)	2.1 (5)
C14	0.088 (1)	−0.100 (1)	−0.014 (1)	2.1 (5)
C15	0.000 (1)	−0.097 (1)	0.058 (2)	3.1 (5)
C16	−0.026 (1)	−0.093 (1)	0.159 (1)	2.5 (5)
C17	−0.122 (1)	−0.089 (1)	0.233 (1)	3.2 (5)
C18	−0.117 (1)	−0.082 (1)	0.324 (2)	3.2 (5)
C19	−0.022 (1)	−0.085 (1)	0.306 (1)	2.8 (5)
C20	0.013 (1)	−0.088 (1)	0.377 (1)	3.0 (5)
C25	0.075 (1)	−0.113 (1)	0.547 (2)	3.5 (5)
C26	0.030 (2)	−0.193 (1)	0.577 (2)	6.7 (7)
C27	0.294 (1)	−0.122 (1)	0.445 (2)	3.6 (5)
C28	0.324 (2)	−0.206 (2)	0.438 (2)	7.8 (8)
C29	0.544 (1)	−0.112 (1)	0.070 (2)	4.7 (6)
C30	0.560 (2)	−0.196 (1)	0.090 (2)	6.5 (7)
C31	0.533 (2)	−0.098 (1)	−0.139 (2)	4.9 (7)
C32	0.557 (1)	−0.176 (1)	−0.188 (2)	5.5 (6)
C33	0.267 (2)	−0.105 (1)	−0.270 (2)	5.0 (7)
C34	0.298 (2)	−0.192 (2)	−0.300 (2)	7.8 (8)
C35	0.046 (1)	−0.117 (1)	−0.163 (2)	4.2 (6)
C36	0.019 (2)	−0.200 (1)	−0.162 (2)	5.9 (6)
C37	−0.205 (1)	−0.097 (1)	0.209 (1)	3.2 (5)
C38	−0.225 (1)	−0.178 (1)	0.196 (2)	4.9 (6)
C39	−0.195 (1)	−0.079 (1)	0.422 (1)	2.8 (5)
C40	−0.220 (2)	−0.155 (1)	0.472 (2)	6.0 (6)
C41	0.200 (1)	0.100 (1)	0.187 (1)	3.1 (5)
C42	0.197 (1)	0.089 (1)	0.289 (1)	3.5 (5)
C100	0.513 (2)	−0.030 (2)	0.568 (3)	11 (1)
C101	0.461 (2)	0.075 (2)	0.521 (3)	12 (1)
C102	0.468 (3)	0.046 (3)	0.617 (3)	14 (1)

[a] Atoms were refined isotropically except the iron atom, which is given in the form of the isotropic equivalent displacement parameter defined as $(4/3)[a^2B(1,1) + b^2B(2,2) + c^2B(3,3) + ab(\cos\gamma)B(1,2) + ac(\cos\beta)B(1,3) + bc(\cos\alpha)B(2,3)]$.

Table V. Main Bond Distances (Å), Angles (deg), and Standard Deviations of (OEP)Fe[$N_4C(CH_3)$]

Fe–N1	2.04 (2)	N5–N8	1.39 (3)
Fe–N2	2.06 (1)	N6–N7	1.38 (3)
Fe–N3	2.02 (2)	N7–N8	1.32 (2)
Fe–N4	2.05 (1)	N5–C41	1.31 (2)
Fe–N5	2.03 (2)	N6–C41	1.34 (2)
C41–C42	1.52 (3)		
N1–Fe–N2	87.2 (6)	N3–Fe–N5	103.0 (6)
N1–Fe–N3	155.1 (6)	N4–Fe–N5	104.6 (5)
N1–Fe–N4	86.2 (7)	N8–N5–C41	110.0 (1)
N1–Fe–N5	101.9 (6)	N7–N6–C41	106.0 (2)
N2–Fe–N3	89.4 (6)	N6–N7–N8	112.0 (2)
N2–Fe–N4	158.1 (5)	N5–N8–N7	101.0 (1)
N2–Fe–N5	97.1 (5)	N5–C41–N6	110.0 (2)
N3–Fe–N4	88.0 (6)	N6–C41–C42	124.0 (2)

Table VI. Infrared Data (ν, cm^{-1}) for the Investigated Complexes (CsI Pellets)

porphyrin, P	axial ligand	$\nu(N_3^-)$		ν(tetrazole)						ν(triazole)			ν(R)			
OEP	N_3^-	2050	2006													
	$N_4C(C_6H_5)$			1448	1360	1160	1125	1053	783				3058	731	508	
	$N_4C(p\text{-}CH_3C_6H_4)$			1447	1358	1161	1121	1031	999				828	823	753	
	$N_4C(m\text{-}CH_3C_6H_4)$			1450	1361	1164		1022					888	797	741	704
	$N_4C(CH_3)$				1360		873	729	705				1090			
	$N_4C(CH_2CH_3)$			1411	1401	1295	1036						1098	1085		
	$N_3C_6H_4$									1300	1243	1157	3059	3020	592	529
TMP	N_3^-	2053	2006													
	$N_4C(C_6H_5)$			1511	1445	1297	1156						3100	758	688	
	$N_4C(CH_3)$				1362			718	698				1096			

Table VII. UV–Visible Data for the (Tetrazolato)- and (Triazolato)iron(III) Porphyrins in Benzene

		λ_{max}, nm (10^{-3} ϵ, M^{-1} cm^{-1})				
		Soret region		Q bands		
porphyrin, P	axial ligand					
OEP	N_3^-	368 (35)	395 (32)	500 (5.4)	527 (5.1)	628 (2.4)
	$N_4C(C_6H_5)$		390 (57)		540 (sh)[a]	590 (sh)
	$N_4C(p\text{-}CH_3C_6H_4)$	360 (sh)	388 (52)		535 (sh)	588 (sh)
	$N_4C(m\text{-}CH_3C_6H_4)$	358 (sh)	393 (52)		536 (sh)	585 (sh)
	$N_4C(CH_3)$		385 (39)		540 (sh)	630 (sh)
	$N_4C(CH_2CH_3)$		387 (38)		535 (sh)	635 (sh)
	$N_3C_6H_4$	358 (sh)	398 (64)		530 (6)	614 (3)
TMP	N_3^-	350 (47)	420 (93)	504 (15)	570 (5.9)	
	$N_4C(C_6H_5)$		415 (121)	512 (15.9)	582 (5.4)	
	$N_4C(CH_3)$	347 (16.8)	412 (56)	508 (5.2)	582 (2.1)	

[a] sh = shoulder.

pancy m = 0.5). The methyl group was not unambiguously located. Except for the methyl hydrogen atoms of the axial ligand and those attached to the solvate molecule, hydrogen atoms were included in calculated positions (C–H = 1.07 Å) and then allowed to ride on the bonded atom with B fixed to 1.3 times those of the corresponding carbon atom. Final difference Fourier synthesis revealed a residual electron density of about 0.3 $Å^{-3}$ near the disordered toluene solvent molecule. Final residuals are given in Table III. Fractional coordinates of the non-hydrogen atoms are given in Table IV, while main bond distances and angles are given in Table V. Other bond distances and angles, anisotropic thermal parameters of the iron atom, hydrogen coordinates, least-squares planes, and structure factors are reported as supplementary material.

Results and Discussion

Characterization of the Tetrazolato and Triazolato Complexes. The synthesis of each Fe(III) complex proceeded as shown in eq 1 where R = C_6H_5, p-$CH_3C_6H_4$, m-$CH_3C_6H_4$, CH_3, or CH_2CH_3.

$$(P)FeN_3 + RCN \rightarrow (P)Fe[N_4C(R)] \qquad (1)$$

Final yields and reaction conditions of each isolated complex are summarized in Table I. The time required to obtain a final product was independent of the porphyrin macrocycle but varied as a function of the specific organic nitrile. The fastest time (15 h) was for aryl dipolarophiles, while the slowest (48–72 h) was for alkyl dipolarophiles. The yields of (OEP)Fe[$N_4C(R)$] varied between 46 and 75%, while those of (TMP)Fe[$N_4C(R)$] varied between 55 (R = CH_3) and 60% (R = C_6H_5). However, neither of the TMP derivatives could be purified due to their high solubility in all solvents, and the listed yield is therefore based on a crude product.

The analytical data are consistent with the calculated molecular formulas.[44] A slow degradation of (P)Fe[$N_4C(R)$] and (P)Fe($N_3C_6H_4$) was noted to occur under aerobic conditions. However, the stability of the σ-bonded tetrazolato and triazolato derivatives was high in solution when under an inert atmosphere and this contrasts with the generally low stability of σ-bonded carbon species of the type (P)Fe(R) under the same experimental conditions.[45-47]

Table VIII. ESR Data for the Investigated Complexes in Toluene at 100 K

porphyrin, P	axial ligand	$g_\perp$	$g_\parallel$[a]
OEP	N_3^-	5.45	2.00 (16.91)
	$N_4C(C_6H_5)$	5.70	2.00 (17.25)
	$N_4C(p\text{-}CH_3C_6H_4)$	5.77	2.01 (17.43)
	$N_4C(m\text{-}CH_3C_6H_4)$	5.61	2.00
	$N_4C(CH_3)$	5.74[b]	2.00[b]
	$N_4C(CH_2CH_3)$	5.58[b]	2.00 (17.16)[b]
	$N_3C_6H_4$	5.87	2.00
TMP	N_3^-	5.41	2.00 (16.74)
	$N_4C(C_6H_5)$	5.77	2.01
	$N_4C(CH_3)$	5.73	2.00

[a] Values in parentheses are coupling constants in Gauss. [b] In 2:1 toluene/methylene chloride mixtures.

Infrared data for the synthesized complexes are reported in Table VI, which also includes data for the starting azido porphyrins, (P)FeN_3. As expected, the N_3^- antisymmetrical vibration of (P)FeN_3 at ≈2000 cm^{-1} is not present in IR spectra of the σ-bonded complexes. Bands typical of tetrazole ring deformations[7-11,26,48-50] appear between 698 and 1511 cm^{-1}, while other bands of (P)Fe[$N_4C(R)$] are attributed to the aryl or alkyl substituent of the bound tetrazole ring. The IR spectrum of the complex formed from (OEP)FeN_3 and benzyne has bands at 1157, 1243, and 1300 cm^{-1}, each of which is assigned as a triazole ring deformation. Four additional vibrations of (OEP)Fe($N_3C_6H_4$) are also listed in Table VI, and these are assigned as due to the benzene ring.

UV–visible data for the investigated complexes in benzene are summarized in Table VII. The spectra of the σ-bonded complexes

(44) Anal. Calcd for (OEP)Fe[$N_4C(C_6H_5)$], $C_{43}H_{49}N_8Fe$: C, 70.3; H, 6.7; N, 15.3. Found: C, 69.7; H, 6.7; N, 15.3. Calcd for (OEP)Fe[$N_4C(CH_3)$], $C_{38}H_{47}N_8Fe$: C, 67.9; H, 7; N, 15.6. Found: C, 67.9; H, 7.2; N, 15.8. Calcd for (OEP)Fe[$N_4C(p\text{-}CH_3C_6H_4)$], $C_{44}H_{51}N_8Fe$: C, 70.6; H, 6.9; N, 14.9. Found: C, 70.0; H, 6.8; N, 14.3.

(45) Cocolios, P.; Lagrange, G.; Guilard, R. *J. Organomet. Chem.* **1983**, *253*, 65.
(46) Guilard, R.; Boisselier-Cocolios, B.; Tabard, A.; Cocolios, P.; Simonet, B.; Kadish, K. M. *Inorg. Chem.* **1985**, *24*, 2509.
(47) Tabard, A.; Cocolios, P.; Lagrange, G.; Gerardin, R.; Hubsch, J.; Lecomte, C.; Zarembowitch, J.; Guilard, R. *Inorg. Chem.* **1988**, *27*, 110.
(48) Jonassen, H. B.; Terry, J. O.; Harris, A. D. *J. Inorg. Nucl. Chem.* **1963**, *25*, 1239.
(49) Holm, R. D.; Donnelly, P. L. *J. Inorg. Nucl. Chem.* **1966**, *28*, 1887.
(50) Garber, L. L.; Sims, L. B.; Brubaker, C. H., Jr. *J. Am. Chem. Soc.* **1968**, *90*, 2518.

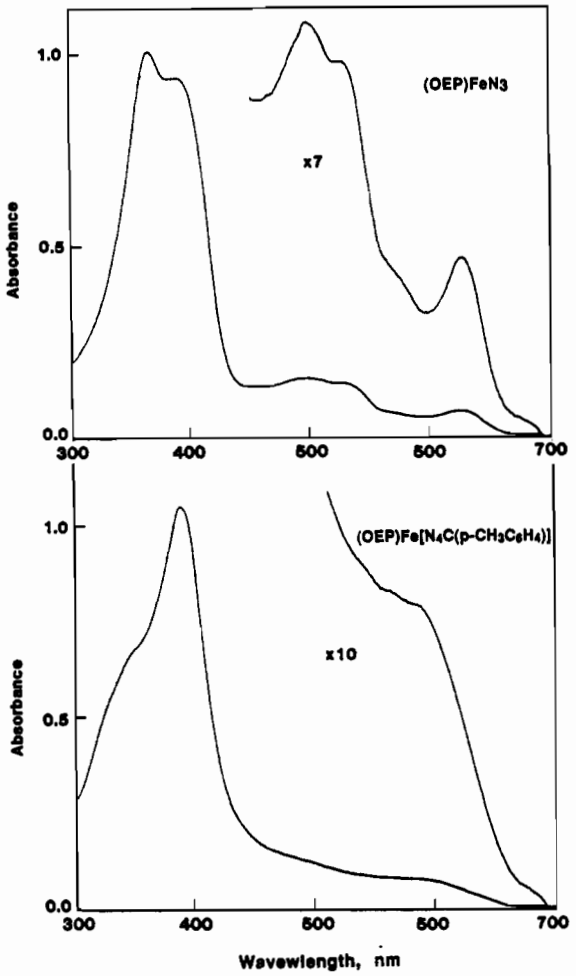

Figure 1. Electronic absorption spectra of (OEP)FeN_3 and (OEP)Fe-[$N_4C(p\text{-}CH_3C_6H_4)$] in C_6H_6.

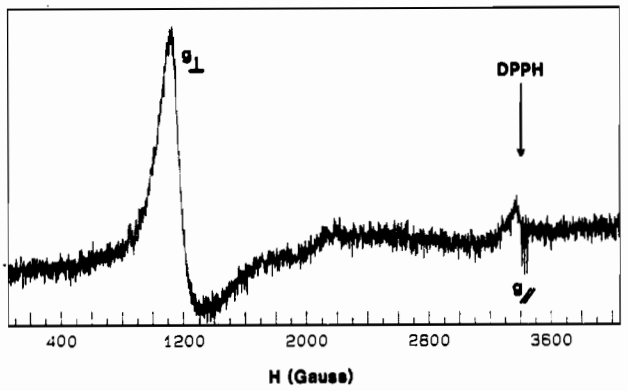

Figure 2. ESR spectrum of (TMP)Fe[$N_4C(C_6H_5)$] at 100 K in toluene.

are all similar to each other but differ from those of (P)FeN_3 under the same solution conditions. This is illustrated in Figure 1 for the case of (OEP)FeN_3 and (OEP)Fe[$N_4C(p\text{-}CH_3C_6H_4)$] in C_6H_6. The Q bands of the tetrazolato complexes are not well resolved and a broad absorption is present in this region (see Table VII and Figure 1). The spectra have some characteristics of high-spin Fe(III) porphyrins, but the exact electronic configuration is not clear-cut due to the lack of an intense Q band that would be observed close to 500 nm for complexes having this spin-state assignment.[51]

The UV–visible spectra of (P)Fe[$N_4C(R)$] indicate that the iron–nitrogen σ bond induces a change in the electronic config-

(51) Gouterman, M. In *The Porphyrins*; Dolphin, D., Ed.; Academic: New York, 1978; Vol. III, Chapter 1.

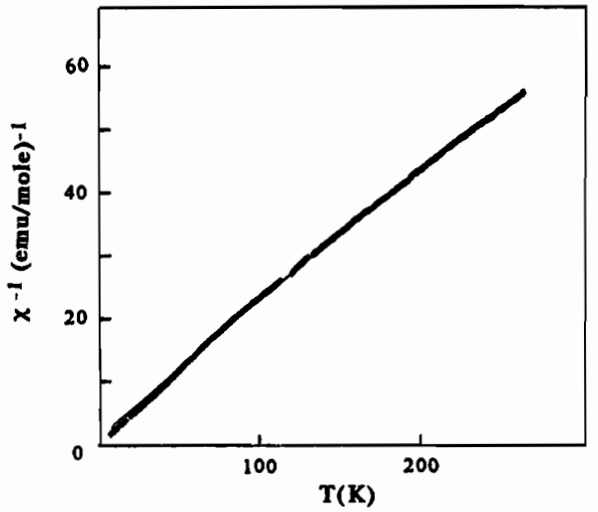

Figure 3. Plot of χ^{-1} vs T for (OEP)Fe[$N_4C(C_6H_5)$].

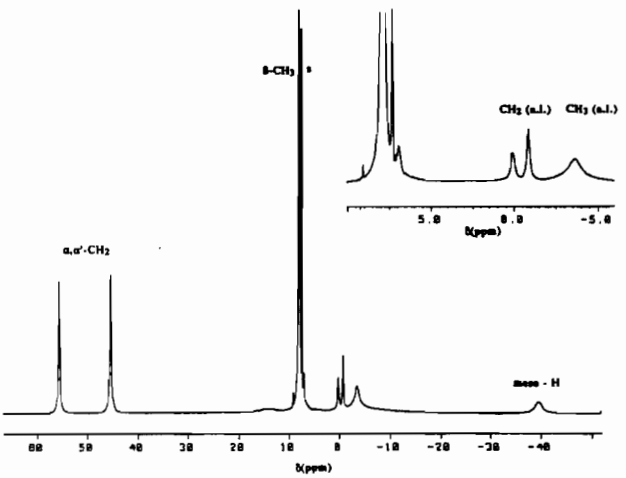

Figure 4. ^1H NMR spectrum of (OEP)Fe[$N_4C(CH_2CH_3)$] at 294 K in $CDCl_3$.

uration with respect to (P)FeN_3, but there are no significant differences in λ_{max} or ϵ of the (P)Fe[$N_4C(R)$] derivatives as a function of the specific σ-bonded axial ligand. This contrasts with iron–carbon σ-bonded complexes of the type (P)Fe(R), all of which have UV–visible spectra that vary significantly with changes in the specific axial ligand.[46]

A summary of ESR spectral data for the investigated complexes is given in Table VIII, while a low-temperature ESR spectrum of (OEP)Fe[$N_4C(C_6H_5)$] is illustrated in Figure 2. All of the spectra are typical of complexes with axial symmetry. The $g_\perp$ signal is associated with a marginally distorted absorption shape away from axial symmetry and shows that there are some rhombic contributions from the ligand field. Each derivative has a low rhombicity, and only two g values could be accurately determined. Nonetheless, all of the ESR spectra are consistent with results expected for high-spin-state iron(III) porphyrins that are complexed with a weak-field axial ligand. These data thus suggest that the electron-withdrawing character of the tetrazolato or triazolato ring will induce a polarization of the iron–nitrogen bond in both (P)Fe[$N_4C(R)$] and (P)Fe($N_3C_6H_4$).

Magnetic susceptibility measurements were performed on two tetrazolato complexes in the solid state between 4 and 300 K at a field strength of 10 kOe. Similar results were obtained for (OEP)Fe[$N_4C(C_6H_5)$] and (OEP)Fe[$N_4C(CH_3)$], and a plot of the inverse molar susceptibility vs temperature is shown in Figure 3 for (OEP)Fe[$N_4C(C_6H_5)$]. There is a linear correlation, and the effective magnetic moment is calculated as 6.26 μ_B. This value is close to the predicted value for a pure high-spin-state Fe(III) complex and is comparable to magnetic values of other well-characterized high-spin Fe(III) porphyrins.[52]

Table IX. ^{1}H NMR Data[a] for the Investigated Complexes

porphyrin, P	axial ligand	R^1	R^2	protons of R^1	multi/intens	δ	protons of R^2	multi/intens	δ	protons of R	multi/intens	δ
OEP	Cl^-	H	CH_2CH_3	meso H	s/4	−56.20	α-CH_2	s/8	40.84			
							α'-CH_2	s/8	44.52			
							β-CH_3	s/24	6.86			
	N_3^-	H	CH_2CH_3	meso H	s/4	−43.98	α-CH_2	s/8	39.44			
							α'-CH_2	s/8	42.14			
							β-CH_3	s/24	6.42			
	$N_4C(C_6H_5)$	H	CH_2CH_3	meso H	s/4	−35.56	α-CH_2	s/8	43.72	ortho H	s/2	5.71
							α'-CH_2	s/8	54.85	meta H	s/2	7.19
							β-CH_3	s/24	7.79	para H	s/1	1.16
	$N_4C(p\text{-}CH_3C_6H_4)$	H	CH_2CH_3	meso H	s/4	−35.43	α-CH_2	s/8	43.51	ortho H	s/2	5.75
							α'-CH_2	s/8	54.81	meta H	s/2	6.88
							β-CH_3	s/24	7.78	para CH_3	s/3	2.60
	$N_4C(m\text{-}CH_3C_6H_4)$	H	CH_2CH_3	meso H	s/4	−31.75	α-CH_2	s/8	42.49	ortho H	s/2	5.80
							α'-CH_2	s/8	55.06	meta H	s/1	6.42
							β-CH_3	s/24	7.80	meta CH_3	s/3	−0.47
										para H	s/1	0.76
	$N_4C(CH_3)$	H	CH_2CH_3	meso H	s/4	−40.08	α-CH_2	s/8	45.28	CH_3	s/3	−0.83
							α'-CH_2	s/8	54.64			
							β-CH_3	s/24	7.74			
	$N_4C(CH_2CH_3)$	H	CH_2CH_3	meso H	s/4	−39.60	α-CH_2	s/8	45.20	α-CH_2	s/1	0.02
							α'-CH_2	s/8	55.49	β-CH_3	s/3	−0.90
							β-CH_3	s/24	7.82			
	$N_3C_6H_4$	H	CH_2CH_3	meso H	s/4	−42.98	α-CH_2	s/8	39.76		s/1	3.33
							α'-CH_2	s/8	42.31		s/1	5.60
							β-CH_3	s/24	6.26		s/1	9.51
											s/1	15.88
TMP	Cl^-	2,4,6-$(CH_3)_3C_6H_2$	H	ortho CH_3	s/12	3.92	pyrrole H	s/8	80.99			
				ortho' CH_3	s/12	6.82						
				meta H	s/4	14.52						
				meta' H	s/4	16.15						
				para CH_3	s/12	4.27						
	N_3^-	2,4,6-$(CH_3)_3C_6H_2$	H	ortho CH_3	s/12	3.36	pyrrole H	s/8	78.56			
				ortho' CH_3	s/12	5.89						
				meta H	s/4	13.09						
				meta' H	s/4	14.19						
				para CH_3	s/12	3.99						
	$N_4C(C_6H_5)$	2,4,6-$(CH_3)_3C_6H_2$	H	ortho CH_3	s/12	3.86	pyrrole H	s/8	60.53	ortho H	s/2	−4.68
				ortho' CH_3	s/12	6.02				meta H	s/2	8.00
				meta H	s/4	14.16				para H	s/1	−2.64
				meta' H	s/4	15.49						
				para CH_3	s/12	4.42						
	$N_4C(CH_3)$	2,4,6-$(CH_3)_3C_6H_2$	H	ortho CH_3	s/12	3.56	pyrrole H	s/8	65.20	CH_3	s/3	−0.19
				ortho' CH_3	s/12	6.38						
				meta H	s/4	14.25						
				meta' H	s/4	15.58						
				para CH_3	s/12	4.22						

[a] Spectra were recorded at 21 °C in $CDCl_3$ with $SiMe_4$ as internal reference; chemical shifts downfield from $SiMe_4$ are defined as positive. Key: R^1 = porphyrin methine group; R^2 = porphyrin pyrrole group; R = axial ligand substituent; s = singlet.

Proton NMR spectra of (OEP)Fe[$N_4C(CH_2CH_3)$] and (TMP)Fe[$N_4C(C_6H_5)$] at 294 K are illustrated in Figures 4 and 5. A summary of the spectral data for these two complexes as well as the other six synthesized derivatives is given in Table IX. The data are typical for high-spin-state Fe(III) porphyrins,[53] and this assignment of the spin state is in agreement with results from ESR and magnetic measurements, both of which have been described above.

The meso proton resonances of (OEP)Fe[$N_4C(R)$] and (OEP)Fe($N_3C_6H_4$) are in the range −31.75 to −42.98 ppm and are at lower fields than corresponding resonances of (OEP)FeN_3 or (OEP)FeCl, which occur at −43.98 and −56.20 ppm, respectively. The β-CH_3 pyrrole groups give a singlet close to 7 ppm. The α-methylene proton signal is located downfield and is split into broad singlets arising from an inequivalence of the two porphyrin faces. This suggests that the iron atom is pentacoordinated and lies above the mean porphyrin plane. The proton diastereotopism is increased by coordination of the tetrazolato or triazolato axial ligand, and this is demonstrated by a large splitting of the methylene proton signal compared to corresponding resonances of (OEP)FeCl or (OEP)FeN_3. Similar effects are not observed in the TMP series, and resonances for *o*-methyl or phenyl meta protons of (TMP)FeN_3 and (TMP)Fe[$N_4C(R)$] are close to each other. This pseudo magnetic equivalence in these com-

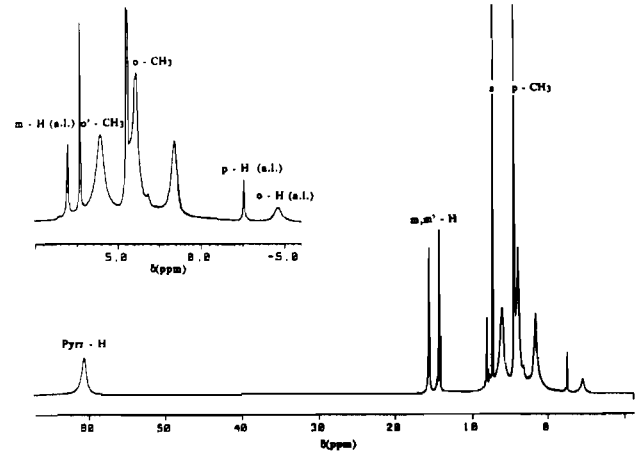

Figure 5. ^{1}H NMR spectrum of (TMP)Fe[$N_4C(C_6H_5)$] at 294 K in $CDCl_3$.

(52) Mitra, S. In *Iron Porphyrins*; Lever, A. B. P., Gray, H. B., Eds.; Addison-Wesley: Reading, MA, 1983; Part II, Chapter 1.
(53) La Mar, G. N.; Walker, F. A. In *The Porphyrins*; Dolphin, D., Ed.; Academic: New York, 1979; Vol. IV, Chapter 2.

plexes may be due to a ring rotation of the bulky mesityl groups in solution.

The pyrrole proton resonance of (TMP)Fe[$N_4C(C_6H_5)$] is located at 60.53 ppm, while that of (TMP)Fe[$N_4C(CH_3)$] is found at 65.20 ppm (see Table IX). Both are typical of high-spin-state Fe(III) species. These resonances appear at higher fields than for (TMP)FeCl or (TMP)FeN_3, and this is due to the higher electron density on the pyrrole and meso sites of the TMP macrocycle. These data also indicate that the iron–nitrogen axial bonds in (TMP)Fe[$N_4C(R)$] are less polarized than the ionic Fe–N_3 or Fe–halide bonds in (P)FeN_3 and (P)FeX. A similar comparison was previously made between Fe(III) porphyrins with anionic axial ligands and those with σ-bonded perfluoroaryl ligands such as in complexes of the type (P)Fe(C_6F_5) or (P)Fe(C_6F_4H).[46]

The axial ligand proton resonances of (P)Fe[$N_4C(R)$] can be assigned both on the basis of relative signal intensity and by comparison with data for all of the tetrazolato complexes. The (P)Fe[$N_4C(R)$] derivatives with aryl R groups have either three or four peaks in the range −0.47 to +7.19 ppm (OEP derivaties) or −4.68–8.00 ppm (TMP derivatives). The large cyclic current of the bulky TMP macrocycle leads to high-field ortho and para proton resonance shifts, and the meta protons are the more deshielded (see Figure 5). The ortho and meta protons of the axial ligand are equivalent, and this can be accounted for by the absence of significant hindered rotation of the bulky mesityl groups. This is unexpected and has not previously been reported for any other TMP derivatives. An alternate interpretation is that the two proton sites are accidently equivalent, but an exact explanation is unknown at this time.

The ^1H NMR spectrum of (OEP)Fe($N_3C_6H_4$) has four peaks located between 3.33 and 15.88 ppm, all of which can be attributed to the triazole ring protons. However, an exact assignment of these resonances is not clear-cut. As expected, the range of ligand resonances for the paramagnetic Fe(III) triazolato complexes is larger than that of the analogous diamagnetic In(III) triazolato porphyrin derivatives (see ref 26) but the overall ^1H NMR spectra of the two compounds are still quite similar. This should only occur if the same type of isomer is obtained for an Fe(III) and In(III) porphyrin with the same triazolato ligand in the Fe and In series.

The OEP and TMP meso and pyrrole proton chemical shifts should depend upon the specific site for tetrazolato substitution but would not vary significantly for complexes where the substitution occurred at the same position on the tetrazolato ligand. As seen in Table IX, the porphyrin proton resonances of the alkyl-substituted tetrazolato complexes are shielded by about 5.0 ppm compared to those of the aryl-substituted derivatives. This difference in chemical shifts can only be explained by different substitution sites on the tetrazolato ligand (see Chart I). However, the ^1H NMR data cannot definitively prove the structure of a given complex, and the exact position of the alkyl or aryl group on the tetrazolato ligand must therefore be determined by X-ray diffraction.

Molecular Configuration of (OEP)Fe[$N_4C(C_6H_5)$] and (OEP)Fe[$N_4C(CH_3)$]. As indicated in the Experimental Section, (OEP)Fe[$N_4C(C_6H_5)$] is isomorphous with the corresponding indium complex, (OEP)In[$N_4C(C_6H_5)$].[25] The methyl group of (OEP)Fe[$N_4C(CH_3)$] is at the 5-position of the tetrazolato ring and is sterically unhindered, as shown in Figure 6. This is not the case for (OEP)Fe[$N_4C(C_6H_5)$], which has the phenyl group located at the 4-position of the tetrazolato ring.

The crystal structure of (OEP)Fe[$N_4C(CH_3)$] is similar to that of (OEP)In[$N_4C(CH_3)$];[26] the iron atom is coordinated to the five nitrogen atoms, and the Fe–N bond lengths are almost equal ($\langle$Fe–N$\rangle$ = 2.04 (2) Å). The metal atom lies 0.412 (2) Å above the plane of the four porphyrin nitrogens, and this geometry is consistent with the presence of a high-spin-state iron(III) central metal.[54] Also, the doming character of (OEP)Fe[$N_4C(CH_3)$] is very small (0.04 Å) compared to that of the In(III) analogue (0.12 Å), (OEP)In[$N_4C(CH_3)$].

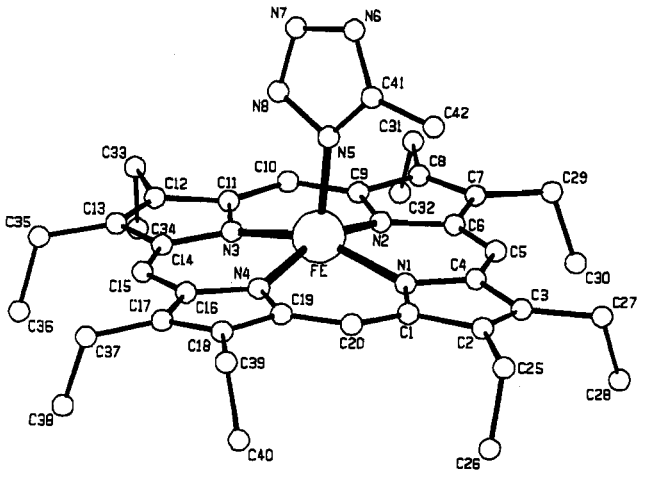

Figure 6. View of (OEP)Fe[$N_4C(CH_3)$].

Chart II

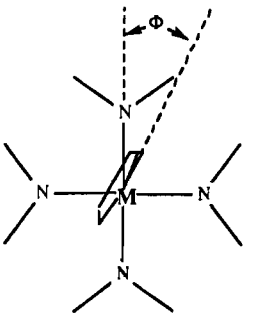

The tetrazolato ligand of (OEP)Fe[$N_4C(CH_3)$] is rigorously planar and tends toward an eclipsed conformation with respect to the two opposite nitrogen atoms (N1, N3) of the porphyrin core: the ϕ angle, as introduced by Hoard,[55] is 12° (see Chart II).

The minimum steric hindrance is achieved for a ϕ angle of 45°, which corresponds to a full staggered conformation. The low value for (P)Fe[$N_4C(CH_3)$] might possibly be explained by electronic effects such as would occur for metal dπ–tetrazolato pπ bonding. However, small ϕ values were also observed for the two investigated indium tetrazolato complexes (ϕ = 8.2° for (OEP)In[$N_4C(CH_3)$] and ϕ = 23.9° for (OEP)In[$N_4C(C_6H_5)$],[26] both of which have a forbidden interaction with filled d orbitals. This suggests that results for the three structurally characterized tetrazolato derivatives should be compared to those of the pentacoordinated (P)M(Im) species[56] where P = OEP, TPP, or TPivP, Im = imidazole, and M = Mn(II), Co(II), Fe(II), or Fe(III). These latter metalloporphyrins have a statistical average angle of 10.4°, with an estimated standard deviation of 7.3°. The average angle was ascertained to be independent of the electronic configuration as well as independent of the spin or oxidation state of the central metal, and this was explained on the basis of charge-iterative extended Hückel calculations.[56] Surprisingly, several of the complexes with different orientation angles have a mean π-bonding interaction between the metal and the imidazole ligand that is mainly dominated by a pπ-pπ interaction. A similar interaction may also be present in (OEP)In[$N_4C(R)$][26] and (OEP)Fe[$N_4C(CH_3)$], as suggested by the structural data.

Electroreduction of (P)Fe[$N_4C(R)$]. Figure 7 illustrates cyclic voltammograms for electroreduction of four representative (OEP)Fe[$N_4C(R)$] complexes in CH_2Cl_2, 0.1 M (TBA)ClO_4. Two of the derivatives contain an alkyl-substituted tetrazolato ligand, while the other two contain an aryl-substituted ligand. The

(54) Scheidt, W. R.; Gouterman, M. In *Iron Porphyrins*; Lever, A. B. P., Gray, H. B., Eds.; Addison-Wesley: Reading, MA, 1983; Part I, Chapter 2.

(55) Collins, D. M.; Countryman, R.; Hoard, J. L. *J. Am. Chem. Soc.* **1972**, *94*, 2066.

(56) Scheidt, W. R.; Chipman, D. M. *J. Am. Chem. Soc.* **1986**, *108*, 1163.

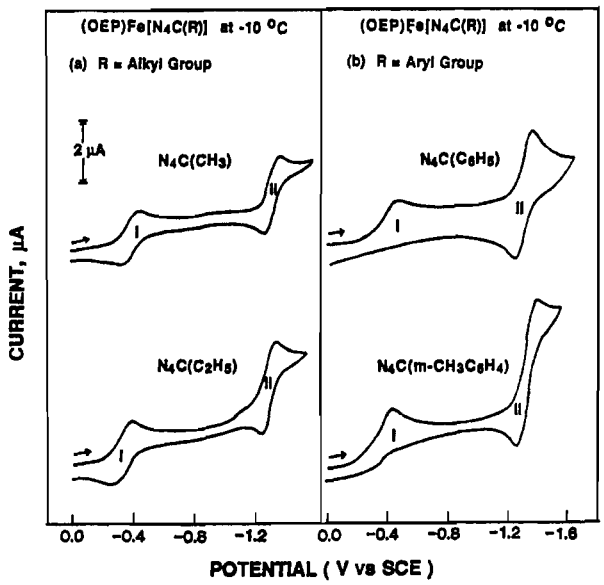

Figure 7. Cyclic voltammograms of (OEP)Fe[$N_4C(R)$] in CH_2Cl_2 containing 0.05 M (TBA)PF_6 at −10 °C where (a) R = CH_3 or CH_2CH_3 and (b) R = C_6H_5 or *m*-$CH_3C_6H_4$.

Scheme I

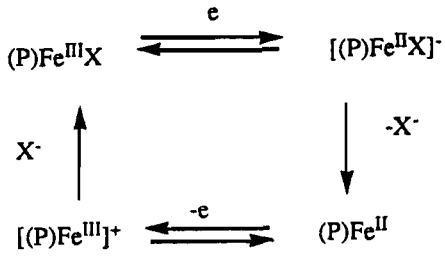

crystallographic data indicate that the CH_3 group of (OEP)Fe[$N_4C(CH_3)$] is substituted in the 5-position of the ring (i.e. isomer I) while the C_6H_5 group of (OEP)Fe[$N_4C(C_6H_5)$] is located at the 4-position of the ring (i.e. isomer II). The former metalloporphyrin undergoes a reversible first reduction at room temperature (see Figure 7a), and this contrasts with the first reduction of (OEP)Fe[$N_4C(C_6H_5)$] (Figure 7b), which is irreversible at all temperatures between +25 and −50 °C.

Irreversible reductions also occur for (OEP)Fe[$N_4C(R)$] where R = *m*-$CH_3C_6H_4$ (Figure 7b) and *p*-$CH_3C_6H_4$ but not for (OEP)Fe[$N_4C(C_2H_5)$] (Figure 7a), which undergoes a reversible reduction under the same experimental conditions. This similarity in the electrochemistry of complexes with a given type of ligand substitution (alkyl or aryl groups) may be due to a different mode of ligand binding (i.e. an isomer effect) or alternatively to different basicities for the two types of tetrazolato ligands. However, in either case, the electrochemical data in Figure 7 could suggest that the CH_2CH_3 group of (OEP)Fe[$N_4C(CH_2CH_3)$] is substituted at the 5-position of the tetrazolato ring (isomer I) while the *m*-$CH_3C_6H_4$ or *p*-$CH_3C_6H_4$ group of (OEP)Fe[$N_4C(R)$] is substituted at the 4-position of the σ-bonded ligand (isomer II). This assignment is also implied by the NMR data in Table IX.

An irreversible Fe(III) → Fe(II) reaction has been reported to occur for all previously investigated (TMP)FeX complexes as well as for numerous (P)FeX derivatives with other porphyrin rings and weak-field anionic axial ligands.[57-62] This irreversibility is associated with a rapid loss of the axial ligand after a reversible electron transfer, as shown in eq 2.

$$(P)FeX + e \rightleftarrows [(P)FeX]^- \rightarrow (P)Fe + X^- \qquad (2)$$

The electrogenerated Fe(II) porphyrin is stable under an inert N_2 atmosphere. However, this species can be reoxidized at more positive potentials, after which the product rapidly associates with a counterion of the supporting electrolyte, as shown by the overall reaction sequence given in Scheme I. Examples for the above oxidation/reduction mechanism are numerous for iron(III) complexes with weak-field axial ligands such as Br^- or Cl^- but not for porphyrins with stronger field ligands such as OH^-, F^-, or OCH_3^-.[57-61]

Similar electrochemical behavior is obtained for reduction of the two investigated (TMP)Fe[$N_4C(R)$] derivatives as well as for (OEP)Fe[$N_4C(R)$] where R = C_6H_5, *m*-$CH_3C_6H_4$, or *p*-$CH_3C_6H_4$. An example of the resulting thin-layer voltammogram is given in Figure 8 for (TMP)Fe[$N_4C(C_6H_5)$], and a summary of the first reduction potentials for each of the complexes in CH_2Cl_2 is given in Table X. The voltammogram in Figure 8 is virtually identical with those for reduction and reoxidation of (TPP)FeBr in CH_2Cl_2 or DMF[57,58,60] and suggests that the σ-bonded (P)Fe[$N_4C(R)$] complexes have properties quite close to those of the five-coordinate high-spin (P)FeBr derivatives. A comparison of half-wave potentials for the reversible first reduction of different (OEP)FeX and (OEP)FeL complexes is given in a following section of the paper and also suggests this analogy.

It has already been noted that the first reduction of (OEP)Fe[$N_4C(R)$], where R = an aryl group, remains irreversible at all temperatures between +25 and −50 °C. A similar irreversibility

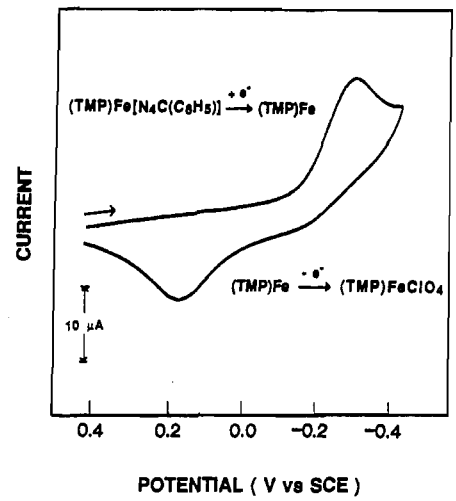

Figure 8. Thin-layer cyclic voltammogram of (TMP)Fe[$N_4C(C_6H_5)$] in CH_2Cl_2 containing 0.2 M (TBA)ClO_4. Scan rate = 10 mV/s.

Table X. Peak Potentials (V) for the First Oxidation and First Reduction of the Tetrazolato Complexes at a Platinum Electrode in CH_2Cl_2[a] (Scan Rate = 0.1 V/s)

porphyrin	axial ligand	E_p (1st oxidn)	E_p (1st redn)
TMP	N_3^-	1.12	−0.56
	$N_4C(CH_3)$	1.02[b]	−0.30[b]
	$N_4C(C_6H_5)$	0.98	−0.34
OEP	N_3^-	1.01	−0.62
	$N_4C(CH_3)$	1.02	−0.32[c]
	$N_4C(CH_2CH_3)$	1.02	−0.37[c]
	$N_4C(C_6H_5)$	0.90	−0.38
	$N_4C(p\text{-}CH_3C_6H_4)$	0.88	−0.34
	$N_4C(m\text{-}CH_3C_6H_4)$	0.91	−0.40

[a] Supporting electrolyte for TMP complexes is 0.2 M (TBA)ClO_4 and for OEP complexes is 0.05 M (TBA)PF_6. [b] Values obtained at a gold working electrode. [c] Reversible $E_{1/2}$ value.

(57) Kadish, K. M. *Prog. Inorg. Chem.* **1986**, *34*, 435.
(58) Kadish, K. M. In *Iron Porphyrins*; Lever, A. B. P., Gray, H. B., Eds.; Addison-Wesley: Reading, MA, 1983; Part II, pp 161-249.
(59) Kadish, K. M.; Bottomley, L. A.; Kelly, S.; Schaeper, D.; Shiue, L. R. *Bioelectrochem. Bioenerg.* **1981**, *8*, 213.
(60) Bottomley, L. A.; Kadish, K. M. *Inorg. Chem.* **1981**, *20*, 1348.
(61) Swistak, C.; Mu, X. H.; Kadish, K. M. *Inorg. Chem.* **1987**, *26*, 4360.
(62) Kadish, K. M.; Rhodes, R. K. *Inorg. Chem.* **1983**, *22*, 1090.

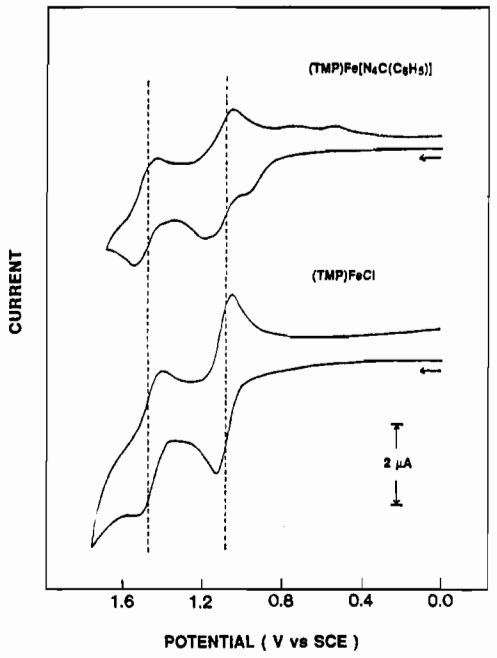

Figure 9. Cyclic voltammograms for the room-temperature oxidation of (TMP)Fe[$N_4C(C_6H_5)$] and (TMP)FeCl in CH_2Cl_2 containing 0.2 M (TBA)ClO_4.

occurs for (TMP)Fe[$N_4C(C_6H_5)$] and (TMP)Fe[$N_4C(CH_3)$] over this temperature range, and these results are consistent with an extremely rapid loss of the axial ligand after formation of an Fe(II) derivative.

The second reduction of (P)Fe[$N_4C(R)$] leads to an Fe(I) complex that rapidly reacts with CH_2Cl_2. This results in an irreversible second process that has an increased cathodic peak current and appears to be catalytic. This type of reaction has been noted for several reduced iron porphyrin derivatives in CH_2Cl_2 at room temperature[57,58,63] but does not occur in coordinating solvents or at lower temperatures where the rate of reaction with the solvent is slowed down sufficiently so that it is not observed on the cyclic voltammetry time scale. For this reason, the voltammograms in the present study were generally measured at −10 °C and under these conditions give a reversible second reduction. This is illustrated in Figure 7 for the four (OEP)Fe[$N_4C(R)$] complexes. At −10 °C, the tetrazolato complexes with P = TMP are reduced at $E_{1/2} = -1.23 \pm 0.2$ V while those with P = OEP are reduced at $E_{1/2} = -1.30 \pm 0.02$ V. Both sets of values are independent of the initial σ-bonded ligand and are within experimental error of literature $E_{1/2}$ values for reduction of (TMP)Fe[61] or (OEP)Fe[57,58] in CH_2Cl_2 containing 0.1 M (TBA)ClO_4.

Electrooxidation of (P)Fe[$N_4C(R)$]. The cyclic voltammograms for oxidation of the five investigated tetrazolato complexes are all self-consistent and indicate a rapid loss of the σ-bonded axial ligand after abstraction of one electron from the complex. An example of these voltammograms is shown in Figure 9 for the case of (TMP)Fe[$N_4C(C_6H_5)$] in CH_2Cl_2, 0.2 M (TBA)ClO_4, and values of E_p for the first oxidation of each tetrazolato derivative are summarized in Table X.

The first oxidation of (TMP)Fe[$N_4C(C_6H_5)$] is irreversible and occurs at $E_p = 0.98$ V for a scan rate of 0.1 V/s. The second and third oxidations are both reversible and are located at $E_{1/2} = 1.10$ and 1.49 V, as shown in Figure 9. Both $E_{1/2}$ values are within experimental error of values obtained for the stepwise ring-centered oxidations of (TMP)$FeClO_4$[61] or (TMP)FeCl (see Figure 9) under the same experimental conditions. This is consistent with a loss of the tetrazolato ligand upon electrooxidation and the rapid conversion of [(TMP)Fe[$N_4C(R)$]]$^{+\bullet}$ to [(TMP)Fe]$^+$, as shown in Scheme II.

Scheme II

$$(TMP)Fe[N_4C(R)] - e \rightleftarrows (TMP)Fe[N_4C(R)]^{+\bullet} \rightarrow [(TMP)Fe]^+ + N_4C(R)^\bullet$$

$$[(TMP)Fe]^+ \rightleftarrows [(TMP)Fe]^{2+} + e$$

$$[(TMP)Fe]^{2+} \rightleftarrows [(TMP)Fe]^{3+} + e$$

Electrooxidation of the five investigated (OEP)Fe[$N_4C(R)$] derivatives also results in a cleavage of the σ-bonded ligand, and an irreversible first oxidation is invariably obtained, even under conditions of low temperature and rapid potential sweep rate. The peak potential for this process ranges between +1.02 and +0.88 V for a scan rate of 0.1 V/s (see Table X), and these values may be compared to a measured E_p of 1.01 V for electrooxidation of (OEP)FeN_3 in CH_2Cl_2 at the same potential sweep rate.

The effect of counterion on half-wave potentials for electrooxidation of various (P)FeX derivatives has been extensively investigated by the groups of Goff[64] and Kadish.[60] The measured $E_{1/2}$ values are independent of the anionic axial ligand when the oxidation occurs at the porphyrin π ring system,[64] but shifts in potential will occur when an Fe(IV) oxidation state is accessed. For example, (OEP)FeX where X = F^-, Cl^-, Br^-, ClO_4^-, and SO_4^{2-} are all oxidized in the range 1.00–1.03 V, and each electrode reaction generates a porphyrin π cation radical.[64] In contrast, the electrooxidations of (P)$FeOCH_3$, (P)FeOH, (P)FeF_2^-, and (P)Fe(R) all occur at more negative potentials,[61,65–68] and the electrogenerated product in each case is assigned as a high-oxidation-state Fe(IV) porphyrin derivative.

As shown in Scheme II the electrooxidation of (P)Fe[$N_4C(R)$] is irreversible due to a rapid loss of the oxidized tetrazolato ligand following electron transfer. This results in the expected negative shift of E_p away from the reversible $E_{1/2}$ value that would be obtained in the absence of a chemical reaction.[69] This shift in E_p is especially evident for the three complexes with aryl-substituted tetrazole rings, all of which undergo a rapid loss of the ligand and thus are more easily oxidized. On the other hand, the two oxidized complexes with alkyl-substituted ligands are slightly more stable in that they undergo a slower decomposition. These complexes both have an oxidation peak at 1.02 V for a scan rate of 0.1 V/s, and this potential compares to a theoretical $E_p = 1.04$ V for a reversible reaction centered at $E_{1/2} = 1.01$ V ($E_{pa} - E_{pc} \approx 60$ mV).[59]

Finally, it is interesting to note that the electrochemical behavior of (P)Fe[$N_4C(R)$] is very similar to that for derivatives of the type (P)M(R) where R is a σ-bonded alkyl or aryl ligand and M is Al,[70] Ga,[71] or In.[72] The first oxidation of these main-group metalloporphyrins is accompanied by cleavage of the metal–carbon σ bond. This results in a generation of [(P)M]$^+$, which then undergoes two additional electron abstractions at the porphyrin π ring system. The voltammogram of (TMP)Fe[$N_4C(C_6H_5)$] in Figure 9 is virtually identical with voltammograms observed for (P)M(R), with the only exception being two small reduction peaks located between 1.0 and 0.6 V on the return potential scan. These processes were not investigated in this present study. However, it is noted that they are not observed on initial oxidative scans

(63) Walker, F. A.; Barry, J. A.; Balke, V. L.; McDermott, G. A.; Wu, M. Z.; Linde, P. F. *Adv. Chem. Ser.* **1983**, *201*, 377.

(64) Philippi, M. A.; Shimomura, E. T.; Goff, H. M. *Inorg. Chem.* **1981**, *20*, 1322.

(65) Groves, J. T.; Gilbert, J. A. *Inorg. Chem.* **1986**, *25*, 123.

(66) (a) Calderwood, T. S.; Lee, W. A.; Bruice, T. C. *J. Am. Chem. Soc.* **1985**, *107*, 8272. (b) Calderwood, T. S.; Bruice, T. C. *Inorg. Chem.* **1986**, *25*, 3722. (c) Lee, W. A.; Calderwood, T. S.; Bruice, T. C. *Proc. Natl. Acad. Sci. U.S.A.* **1985**, *82*, 4301.

(67) Hickman, D. L.; Goff, H. M. *Inorg. Chem.* **1983**, *22*, 2787.

(68) Lançon, D.; Cocolios, P.; Guilard, R.; Kadish, K. M. *J. Am. Chem. Soc.* **1984**, *106*, 4472.

(69) Nicholson, R. S.; Shain, I. *Anal. Chem.* **1964**, *36*, 706.

(70) Guilard, R.; Zrineh, A.; Tabard, A.; Endo, A.; Han, B. C.; Lecomte, C.; Souhassou, M.; Habbou, A.; Ferhat, M.; Kadish, K. M. *Inorg. Chem.* **1990**, *29*, 4476.

(71) Kadish, K. M.; Boisselier-Cocolios, B.; Coutsolelos, A.; Mitaine, P.; Guilard, R. *Inorg. Chem.* **1985**, *24*, 4521.

(72) Kadish, K. M.; Boisselier-Cocolios, B.; Cocolios, P.; Guilard, R. *Inorg. Chem.* **1985**, *24*, 2139.

Table XI. Separation of Isotropic Shifts[a] into Contact and Dipolar Contributions of (OEP)FeX and (OEP)Fe[$N_4C(R)$] Complexes (in $CDCl_3$ at 294 K)

compd	proton type	$(\Delta H/H)_{iso}$, ppm	$(\Delta H/H)_{dip}$, ppm	$(\Delta H/H)_{con}$, ppm	geometric[b] factor, Å^3	A/h, 10^5 Hz	D, cm^{-1}
(OEP)FeCl	α-CH_2	36.66	5.79	30.87	−0.0038[c]	1.00	≈8[d]
	α′-CH_2	40.34	5.79	34.55	−0.0038[c]	1.10	
	β-CH_3	4.88	4.11	0.77	−0.0027[c]	0.03	
	meso H	−66.57	16.14	−82.71	−0.0106[c]	−2.70	
(OEP)FeN_3	α-CH_2	35.24	4.92	30.32	−0.0038[c]	0.99	≈6
	α′-CH_2	37.94	4.92	33.02	−0.0038[c]	1.08	
	β-CH_3	4.44	3.50	0.94	−0.0027[c]	0.03	
	meso H	−54.36	13.73	−68.09	−0.0106[c]	−2.22	
(OEP)Fe[$N_4C(C_6H_5)$]	α-CH_2	39.60	14.85	24.75	−0.0039	0.81	≈10
	α′-CH_2	50.60	14.85	35.75	−0.0039	1.17	
	β-CH_3	5.84	9.90	−4.06	−0.0026	−0.13	
	meso H	−45.92	46.84	−92.76	−0.0123	−3.03	
	ortho H	−0.93	−25.51	24.58	0.0067	0.80	
	meta H	1.01	−10.28	11.29	0.0027	0.37	
	para H	−5.02	−8.38	3.36	0.0022	0.11	
(OEP)Fe[$N_4C(CH_3)$]	α-CH_2	41.10	7.67	33.43	−0.0039	1.09	≈8
	α′-CH_2	50.46	7.67	42.79	−0.0039	1.40	
	β-CH_3	5.78	5.12	0.66	−0.0026	0.02	
	meso H	−50.49	24.20	−74.69	−0.0123	−2.44	
	CH_3	0.27	−13.58	13.85	0.0069	0.45	

[a] Referenced against analogous diamagnetic indium(III) complexes in $CDCl_3$. [b] Axial geometric factor $\langle(3\cos^2\theta - 1)r^{-3}\rangle_{av}$. [c] Data from refs 75 and 76. [d] Data from ref 77.

and are most likely due to a reduction of the oxidized tetrazolato ligand or to a product resulting from a chemical reaction of this oxidized ligand in solution.

Electronic Structure of Tetrazolato Complexes and Relative Ligand Field Strength. A knowledge of structural parameters permits one to determine the electronic structure of the tetrazolato complexes and to compare their electronic properties with those of other well-characterized high-spin-state iron(III) porphyrins. The proton isotropic shifts of the OEP derivatives are summarized in Table XI and were calculated by comparison with the analogous In(III) tetrazolato derivatives.[26] Dipolar shifts were calculated by analyzing the curvature in the Curie plot, and this was done in order to determine the contact contributions of the isotropic shifts.

These isotropic shifts vs temperature are shown in Figure 10 for (OEP)Fe[$N_4C(CH_3)$] in $CDCl_3$. According to the theory of Kurland and McGarvey,[73] the isotropic shift for a high-spin iron(III) complex can be given as follows:

$$\left(\frac{\Delta H}{H}\right)_{iso} = \left(\frac{\Delta H}{H}\right)_{con} + \left(\frac{\Delta H}{H}\right)_{dip} = -\left(\frac{A}{h}\right)\frac{C}{T} + B\frac{3\cos^2\theta - 1}{r^3}\frac{D}{T^2}$$

where A/h is the Fermi coupling constant, T is the absolute temperature, $C = 35g\beta/(12k(\gamma H/2\pi)$ (β = Bohr magneton, k = Boltzmann's constant, and g/H = proton magnetogyric ratio), $B = 28g^2\beta^2/9k^2$, $(3\cos^2\theta - 1)/r^3$ is the geometric factor, and D is the zero-field-splitting parameter (ZFS). The Fermi coupling constants and the ZFS parameters can be calculated by fitting the experimental points and calculating the geometric factors from structural data. These values are reported in Table XI. It was assumed in these calculations that the complexes have the same anisotropy in solution and in the solid state. The resulting data are all close to values reported for (OEP)FeCl and (OEP)FeN_3 and are consistent with a high-spin-state iron(III) center in the cases.

The D parameter of (TPP)FeCl has been accurately determined by single-crystal susceptibility measurements[74] and the B and C constants of (OEP)Fe[$N_4C(C_6H_5)$] and (OEP)Fe[$N_4C(CH_3)$] were corrected by using the Curie plot data for this compound. These fitted isotropic shift data gave the D and A/h parameters for the tetrazolato complexes based on the corrected B and C constants.

The zero-field splitting increases according to the nature of the axial ligand and follows in the order $D_{N_3^-} < D_{Cl^-} \approx D_{N_4C(CH_3)} < D_{N_4C(C_6H_5)}$. The lower the D value, the lower is the field of the axial ligand. Magnetization anisotropy measurements were not made, and it was not possible to determine the crystal-field parameters. However, the results of this study confirm that the iron–nitrogen bond in (P)Fe[$N_4C(R)$] is slightly covalent. These data also show that the ligand field strength of $N_4C(C_6H_5)$ is higher than that of $N_4C(CH_3)$, due perhaps to the different substitution sites of the two tetrazole rings.

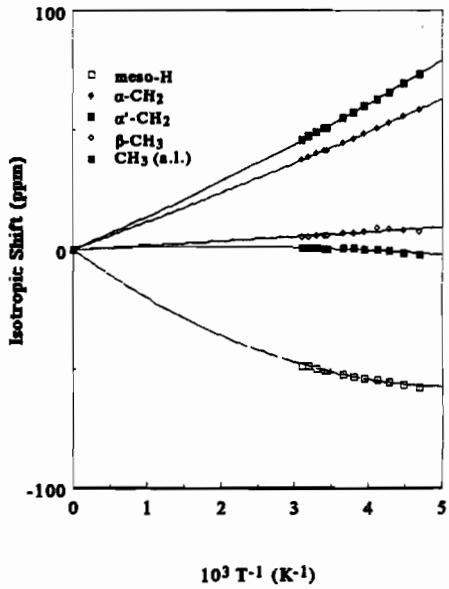

Figure 10. Temperature dependence for isotropic shifts of (OEP)Fe[$N_4C(CH_3)$] in $CDCl_3$.

The shift of each proton site possesses a large dipolar contribution, even in the case of (P)Fe[$N_4C(R)$] complexes with aryl group substituents. The largest dipolar contribution to the axial aryl proton isotropic shifts is observed for the para protons. The absolute values of the contact and pseudocontact shifts of the other tetrazolato group protons are close to each other and the contact shifts of the axial aryl protons follow the sequence

$$\left(\frac{\Delta H}{H}\right)_{con}(\text{ortho H}) > \left(\frac{\Delta H}{H}\right)_{con}(\text{meta H}) > \left(\frac{\Delta H}{H}\right)_{con}(\text{para H})$$

Calculated Fermi coupling constants are summarized in Table XI. These constants show that the σ spin density on the pyrrole sites is due to a σ donation of the nitrogen lone pair toward the

(73) Kurland, R. J.; McGarvey, B. R. *J. Magn. Reson.* **1970**, *2*, 286.
(74) Behere, D. V.; Birdy, R.; Mitra, S. *Inorg. Chem.* **1981**, *20*, 2786.

Table XII. Reduction Potentials (V vs SCE) of Various Five-Coordinated Fe(III) Octaethylporphyrin Complexes in CH_2Cl_2 Containing (TBA)ClO_4 or (TBA)PF_6 as Supporting Electrolyte

axial ligand	type of bond	spin state[a]	$E_{1/2}$	ref
ClO_4^-	ionic	is, hs	0.10	59
$N_4C(C_2H_5)$	σ	hs	-0.32	this work
Br^-	ionic	hs	-0.34	59
$N_4C(CH_3)$	σ	hs	-0.37	this work
Cl^-	ionic	hs	-0.42	59
N_3^-	ionic	hs	-0.52	this work
F^-	ionic	hs	-0.63	59
C_6F_4H	σ	hs	-0.64[b]	46
C_6F_5	σ	hs	-0.66[b]	46
C_6H_5	σ	ls	-0.91	68

[a] Key: is = intermediate spin; hs = high spin; ls = low spin. [b] Irreversible reaction. Value listed is E_p at a scan rate of 0.1 V/s.

iron atom, while delocalization of the unpaired electron spin from the d_{xz} and d_{yz} orbitals toward the $4e(\pi^*)$ porphyrin orbitals induces a π spin density on the meso site.[75] The contact shifts of the axial tetrazolato substituents are indicative of a low σ spin density. The magnitude of the contact contribution also appears to be strongly dependent upon the nature of the axial ligand (see Table XI).

In the preceding paper,[26] potentials for electroreduction were used to evaluate the relative metal-ligand bond strength of various (TPP)InX, (TPP)In(R), and (TPP)In[N_4C(R)] complexes. The most easily reduced In(III) porphyrins are those with ionic or tetrazolato axial ligands, while the most difficult to reduce are those with σ-bonded alkyl or aryl axial ligands. The same order is observed for iron(III) porphyrins, but for these complexes the effect of metal spin state must also be considered in evaluating the trends of $E_{1/2}$ with changes in metal-ligand bond strength.

A summary of potentials for reduction of 10 representative pentacoordinated Fe(III) OEP complexes is given in Table XII. Each compound undergoes an Fe(III) → Fe(II) reduction at a potential that is strongly dependent upon the axial ligand field strength as well as upon the spin state of the central metal. The most easily reduced Fe(III) porphyrin is (OEP)FeClO_4 ($E_{1/2}$ = +0.10 V), while the most difficult is (OEP)Fe(C_6H_5) ($E_{1/2}$ = -0.91 V). The perchlorate derivative contains a mixture of intermediate- and high-spin Fe(III), while the σ-bonded phenyl complex is characterized as containing low-spin Fe(III).[68] The remaining compounds in Table XII are all high spin and have $E_{1/2}$ values that shift in the following order: $N_4C(CH_2CH_3) \approx Br^- < N_4C(CH_3) < Cl^- N_3^- < F^- < C_6F_5 < C_6F_4H$.

Correlations between electrochemical data and ^{13}C NMR parameters[78] or Fe(III) binding energies as measured by XPS[79] have been carried out for (TPP)FeX complexes containing the above anionic ligands as well as $OC_6H_5^-$, $O(p\text{-}NO_2C_6H_4)^-$, OAc^-, and NCS^-. The electrochemical data in Table XII are consistent with the order of ligand field strength reported in the literature[78,79] and give further evidence to support an axial anionic-like metal-ligand bond in (P)Fe[N_4C(R)]. The spectroscopic and electrochemical data both indicate that the tetrazolato ligand is weaker than either N_3^- or Cl^-, and this conclusion was also reached by an evaluation of the complexes' zero-field splitting.

Concluding Remarks. This study has demonstrated that it is possible to involve the axial azide of an iron porphyrin in a classical organic reaction. The reactions reported in this paper lead to new series of σ-bonded nitrogen iron derivatives which have never before been reported in iron porphyrin chemistry. The electronic configuration of these tetrazolato and triazolato complexes are close to those of the starting (P)FeN_3 compounds as well as close to those of other (P)FeX derivatives with anionic axial ligands. The iron atoms of (P)Fe[N_4C(R)] and (P)Fe($N_3C_6H_4$) are all in a high-spin state and the axial iron-nitrogen bonds all have a slight covalent character. These compounds model the entry of the active site of cytochrome P-450_{cam} and prove that compounds such as 2-phenylimidazole[37] can inhibit the oxidation of camphor in camphor P-450 with no direct coordination to the heme iron atom.

Acknowledgment. We acknowledge J. Hubsch (Laboratoire de Minéralogie et Cristallographie, Université de Nancy I, France) for the magnetic susceptibility measurements. The support of the CNRS, the National Institutes of Health (K.M.K.; Grant No. GM25172), and Nato (Grant 0168(87)) is also gratefully acknowledged.

Supplementary Material Available: Tables of hydrogen atom fractional coordinates, anisotropic temperature factors, bond distances and angles, and least-squares planes (11 pages); a table of observed and calculated structure factors for (OEP)Fe[$N_4C(CH_3)$] (6 pages). Ordering information is given on any current masthead page.

(75) Walker, F. A.; La Mar, G. N. *Ann. N.Y. Acad. Sci.* **1973**, *206*, 328.
(76) La Mar, G. N.; Eaton, G. R.; Holm, R. H.; Walker, F. A. *J. Am. Chem. Soc.* **1973**, *95*, 63.
(77) Dolphin, D. H.; Sams, J. R.; Tsin, T. B.; Wong, K. L. *J. Am. Chem. Soc.* **1978**, *100*, 1711.
(78) Goff, H. M.; Shimomura, E. T.; Philippi, M. A. *Inorg. Chem.* **1983**, *22*, 66.
(79) Kadish, K. M.; Bottomley, L. A.; Brace, J. G.; Winograd, N. *J. Am. Chem. Soc.* **1980**, *102*, 4341.

Contribution from the Department of Chemistry, University of Alabama, Tuscaloosa, Alabama 35487-0336

Heteronuclear Multiple-Quantum Coherence NMR Spectroscopy of Paramagnetic Heme and Cytochrome *c*-551

Russell Timkovich

Received April 23, 1990

Heteronuclear multiple-quantum coherence (HMQC), heteronuclear multiple-bond coherence (HMBC), and heteronuclear multiple-quantum relay (HMQR) NMR spectra were obtained for the bis(cyano) complex of iron(III) protoporphyrin IX (dicyanoheme *b*), its free base, horse heart ferricytochrome *c*, and *Pseudomonas aeruginosa* ferricytochrome *c*-551. For the heme it was possible to assign all the protons and carbons. For the hemoproteins, it was possible to assign select protons and carbon atoms near the paramagnetic iron that can act as active-site probes in both the ^1H and ^{13}C frequency regions.

Introduction

Cytochrome *c*-551 is an electron-transport protein that functions in bacteria analogously to cytochrome *c* in mitochondrial electron transport. With 82 amino acid residues as opposed to the ca. 103 for the latter cytochrome, it is a structurally simplified version that performs an equivalent function. One approach toward understanding the structure-mechanism relation in cytochromes is to compare properties for the smaller and larger versions. Examination of the paramagnetically shifted NMR spectra of cytochromes has been an important study in general, because the

0020-1669/91/1330-0037$02.50/0